1 **Lateralised contributions of the fusiform cortex to face detection**
2
3 Jessica Taubert[1]*
4 Amanda K. Robinson[1]
5 Jason B. Mattingley[1,2]
6
7 [1] The School of Psychology, The University of Queensland, QLD Australia
8 [2] Queensland Brain Institute, The University of Queensland, QLD Australia
9
10 *Corresponding author
11   Associate Professor Jessica Taubert
12   School of Psychology
13   The University of Queensland
14   St Lucia, Qld 4072 Australia
15   *Email* j.taubert@uq.edu.au

Summary

Neuronal populations in ventral visual cortex are often classified according to the stimuli that elicit their strongest excitatory response. Using such preferred or effective stimuli, receptive fields have been mapped to better understand links between visual responses and behaviour. For example, face-selective regions in human ventral cortex, which prefer faces over objects, are thought to have small, foveally-biased receptive fields, supporting the recognition of subtle facial cues. However, little is known about how face selectivity interacts with stimulus location, or whether selective responses to peripheral faces are altered when competing visual inputs are present. Here, we used ultra-fast 7T fMRI to test whether the Fusiform Face Area (FFA) continues to prefer faces when they occur in the periphery or with competing inputs. We found that face-selective responses in the FFA were robust to competition, whereas object-selective responses in the neighbouring area of the Medial Temporal Lobe (MTL) were reduced. The left FFA showed a contralateral bias that encoded the spatial location of peripheral faces, consistent with a role in orienting toward socially relevant stimuli. In contrast, the right FFA exhibited a stronger category bias that was largely invariant to stimulus position and persisted under competition, suggesting a potential role in evaluating faces prior to fixation. Taken together, these findings reveal lateralised contributions of fusiform cortex to face detection: the left FFA supports the localisation of faces, while the right FFA provides robust categorical information. Together, the findings highlight how the human face-selective network is adapted to detect and prioritise faces under naturalistic viewing conditions.

Highlights

- FFA responses to peripheral faces are robust to competitive inputs
- Left FFA encodes spatial location of peripheral faces with a contralateral bias
- Right FFA shows a strong category bias, invariant to stimulus position

1 Introduction

2 The size and position of neuronal receptive fields have been leveraged to understand the function
3 of discrete visual areas in the primate brain[1-4]. For example, in the face-selective areas of the ventral
4 visual cortex, the majority of neurons have receptive fields that are modest in size (5 – 10 DVA) and
5 foveally-biased[5-8]. These observations have informed theories linking activity in face-selective areas
6 with detailed subordinate-level recognition of facial identity, which is assumed to require fixation[9-12].
7 However, receptive fields are typically mapped by measuring excitatory responses to preferred
8 stimuli. It therefore remains unknown whether the same brain areas continue to prefer faces over
9 objects when stimuli are presented in the visual periphery.

10   A recent neuroimaging study of macaque visual cortex shed some light on this question. In
11 that study, the researchers manipulated the screen location of faces and objects, relative to fixation,
12 as well as the presence of competitive inputs[13] (also see[14-16]). Competitive inputs in this context
13 involved concurrent presentation of adjacent complex scenes. For example, when a face was
14 presented to the left visual field, a pair of scene stimuli were presented centrally (i.e., at the fovea)
15 and in the right visual field[13]. These manipulations revealed that, while face-selective responses
16 survived when peripheral faces were presented in isolation, they were eliminated when peripheral
17 faces were presented alongside competitive inputs. This highlights the importance of testing the
18 tolerance of face-selectivity under conditions that mimic key aspects of naturalistic viewing, in which
19 faces and objects seldom appear in the absence of other stimulus inputs. More importantly, these
20 findings suggested that faces may need to be fixated before they can be distinguished from objects
21 and processed by the cortical face-selective network in the macaque brain[13].

22   Given that faces confer a robust behavioural advantage over objects in a range of spatial
23 detection[17-21] and viewing preference[22-25] tasks, it has been argued that the primate brain *must* be
24 equipped to distinguish faces from objects based on coarse, peripheral input rather than high-fidelity
25 foveal input[26]. Recent work has indicated that the Fusiform Face Area (FFA) may be unique among
26 high-level visual areas in showing a stronger preference for stimulus category than for stimulus
27 location[27]. This raises the possibility that the FFA supports rapid face detection. However, because
28 Silson et al.[27] presented all of their stimuli in isolation, it remains unclear whether the FFA continues
29 to respond preferentially to peripheral faces when competitive inputs are present. Moreover,
30 evidence that the left and right FFA contribute differently to face detection[28-30] highlights the need to
31 test for hemispheric lateralisation.

32   Here we tested whether the human FFA contributes to the rapid face detection using an ultra-
33 fast functional MRI sequence and a high-field scanner (7T Seimens Magnetom). This enabled us to
34 map face-selective activity on the ventral surface of the human brain using a factorial design with
35 three factors; stimulus category (faces vs objects), stimulus position (fovea vs left vs right), and
36 competition (no competition vs competition). We reasoned that if the FFA plays a role in the detection
37 of faces, then the preference for faces over objects in this specific brain region should be robust to
38 the presence of competitive inputs.

Results

Perceived dissimilarity among naturalistic visual stimuli

Although behavioural research has long been dominated by the use of highly controlled face stimuli[31-33], neural responses to face stimuli are typically measured in relation to a different object category, which can be more difficult to control[34-38]. Further, recent theoretical and empirical work has argued that this level of control might inadvertently strip visual stimuli of the image properties, such as colour, that are necessary to understand the processing of faces under naturalistic circumstances[39-44]. Therefore, in this study our goal was to probe the function of the FFA using a stimulus set that included faces, objects and scenes that were rated by participants as belonging to separate stimulus categories, while also being allowed to vary in naturalistic ways. To this end, we collected 180 stimuli and assigned each of them to one of three categories (45 faces, 45 objects, and 90 scenes; see **Fig. 1A**). Amongst our stimuli, "objects" could also be described as "object-oriented scenes" because they were close-ups of objects positioned at the center of the image[45] (**Fig.1A**). The category we labelled as "scenes" could also be described as "scene-oriented scenes" because they were broad perspectives with a visible horizon, but they often also contained objects[45] (**Fig.1A**).

To verify their category assignment, we employed an online triplet odd-one-out task and analysed dissimilarity judgements from 73 adult participants[46]. On each trial, three stimuli were selected at random and presented to the participant. Their task was to select the odd one out, guided by their own interpretation of this instruction (**Fig. 1B**). We collected the responses from 21900 odd-one-out trials and computed the number of times each stimulus was perceived to be the odd one out, compared with the number of times it was presented with every other stimulus, to generate a behavioural Representational Dissimilarity Matrix (RDM[47-49]). This experimental approach not only captures high-level conceptual and semantic information, such as stimulus category, but also more primitive visual distinctions. The approach was therefore ideal for verifying that our stimuli were organised into three categories despite all the ways the stimuli were allowed to vary[49]. We then compared the behavioural RDM (**Fig. 1C**) with a stimulus category model predicting maximum similarity within each category and maximum dissimilarity across categories. We found a significant correlation ($Spearman's\ \rho = 0.52, p < 0.001$), confirming that the stimuli in each of the categories were perceived as more similar to each other than to the stimuli belonging to the other two categories. The clustering of the three stimulus categories is evident in the multidimensional scaling plot (**Fig. 1D**), which visualizes the first two dimensions in the perceptual space. Therefore, we used all 180 stimuli in the subsequent Competition Experiment in the MRI scanner (**Fig. 1E**).
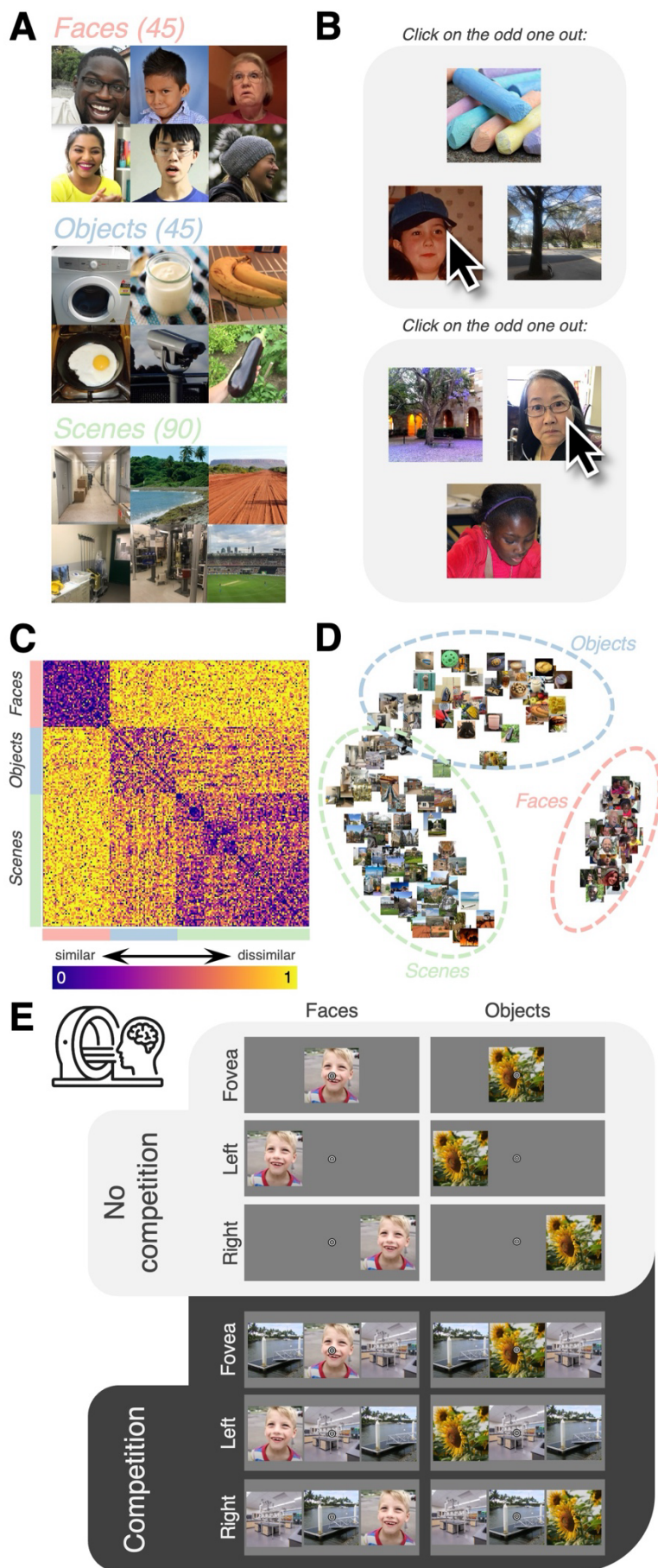
1
2 **Fig. 1. Highly-variable, naturalistic, stimuli were perceived as belonging to three different stimulus categories. (A).**
3 Six examples of the faces (*top*), objects (*middle*) and scenes (*bottom*) selected for the behavioural and brain imaging
4 experiments. **(B).** We employed the triplet odd-one-out similarity task. The triplet odd-one-out task measures object

dissimilarity as the probability of a stimulus being selected as the odd one out. On each trial, participants were shown three stimuli selected at random, and used a computer mouse to select the odd one out. The task evokes different contexts for determining the uniqueness of a stimulus, which in turn emphasizes all behaviourally relevant perceptual dimensions. **(C).** The data from the triplet odd-one-out task were used to construct a 180 x 180 behavioural RDM, reflecting the perceptual dissimilarity between all pairs of stimuli. The colour bar range is scaled to the maximum (1) and minimum (0) of the dissimilarity values. **(D).** Visualization of the behavioural RDM in (c) using multidimensional scaling (MDS). The first two dimensions following MDS are plotted. The proximity of the images represents how similar the stimuli were perceived to be. Dashed lines identify the location of stimuli in each of the three stimulus categories **(E).** Experimental design for the Competition Experiment. Half of the trials contained faces, the other half objects. Face and object stimuli were either presented behind the central fixation spot at the fovea, or they were presented to the left or right visual field. In the no-competition condition, only a face or an object appeared. In the no competition condition, faces and objects appeared with two scenes occupying the remaining spatial locations.

1 Ultra-fast, high-field functional Magnetic Resonance Imaging

2 For the Functional Localizer and the Competition Experiment, we developed an ultra-fast T2*

3 sequence with a TR of 500 ms. This enabled us to implement a 2 x 3 x 2 factorial design with stimulus

4 category (faces vs objects), stimulus position (fovea, left and right), and competition (no competition

5 vs competition present) as repeated factors (**Fig. 1E**). All 12 experimental conditions were presented

6 in an event-related fMRI design; during a run, each face stimulus was seen once in each of the 6

7 unique "face" conditions. Similarly, each object stimulus was seen once in each of the 6 unique

8 "object" conditions (see **Fig. 1E**). In total there were 540 trials per run with trial order determined at

9 random. Since every participant completed 8 runs in total, we collected 4320 trials per participant.

10 For more details see STAR methods.

11

12 Competition does not eliminate sensitivity to peripheral face stimuli in the FFA

13 The Functional Localizer data were used to define four regions of interest at the group level ($N = 20$)

14 in Montreal Neurological Institute (MNI) space; the left FFA, the right FFA, the left object-selective

15 medial temporal lobe (MTL) and the right MTL (for details see STAR methods). We used these masks

16 to perform ROI analyses for the Competition Experiment. To measure sensitivity to the preferred

17 stimulus category (namely, face-selectivity in the FFA), we computed *d'* scores for each ROI, and

18 each participant, using the following formula[50,51]:

19

20
$$d' = \frac{[\bar{\beta}faces - \bar{\beta}objects]}{\sqrt{[\sigma^2 faces + \sigma^2 objects]}\frac{1}{2}}$$

21

22 Given our experimental design, we were able to calculate separate *d'* scores for the foveal

23 presentations of faces and objects, as well as for the contralateral and ipsilateral presentations of

24 faces and objects (see **Fig. 2A,** ***top***). Additionally, we computed separate *d'* scores for the No

25 Competition and Competition conditions. Averaging across hemispheres, this analysis revealed that

26 the sensitivity of the FFA to peripheral face stimuli survived competition from peripheral stimuli, with

27 all average *d'* scores above zero (one sample *t*-tests, all *p*-values < 0.001, Cohen's d values ranged

28 from 1.1 – 0.57; the only exception was the *p*-value associated with ipsilateral presentation in the

29 Competition condition which was higher but still significant, *p* = 0.017, Cohen's *d* = 0.4; **Fig. 2B,** ***left***).

30 There was no evidence that competitive inputs reduced the preference for faces in foveal (paired *t*-

31 test, *t*(39) = 1.2, *p* = 0.24, two-tailed, Cohen's *d* = 0.19), contralateral (paired *t*-test, *t*(39) = 0.07, *p* =

32 0.95, two-tailed, Cohen's *d* = 0.01), or ipsilateral (paired *t*-test, *t*(39) = 1.4, *p* = 0.17, two-tailed,

33 Cohen's *d* = 0.22) regions of the visual field (**Fig. 2B,** ***left***).

34   Next, we probed contralateral biases in the left and right FFA by, first, computing traditional

35 contralateral bias scores by subtracting the response to faces in the ipsilateral visual field from the

36 response to faces in the contralateral visual field when no competition was present (see **Fig. 2A,**

37 ***bottom***). As expected, both the left and right FFA showed preferences for contralateral faces over

38 ipsilateral faces (one sample *t*-tests, two-tailed; left FFA, *t*(19) = 5.34, *p* < 0.001, Cohen's *d* = 1.19;

right FFA, $t(19) = 3.62$, $p = 0.002$, Cohen's $d = 0.81$). The analyses so far provide evidence for face-selectivity regardless of stimulus position, as well as a traditional contralateral bias in FFA responses. However, we were also able to compute contralateral biases as a function of the contrast between faces and objects (see **Fig. 2A, *bottom***). Using this approach, we discovered that the left, but not right, FFA exhibited a face-selective contralateral bias. That is, in left FFA there was a preference for faces over objects that was stronger in the contralateral visual field than the ipsilateral visual field (one sample *t*-test, $t(19) = 2.15$, $p = 0.04$, two-tailed, Cohen's $d = 0.48$; **Fig. 2B, *right***). This bias was also robust to competitive inputs (one sample *t*-test, $t(19) = 2.15$, $p = 0.04$, two-tailed, Cohen's $d = 0.48$; **Fig. 2B, *right***). In contrast, there was no evidence that the right FFA had a preference for faces over objects that differed across visual fields (one sample *t*-tests, two-tailed; No Competition, $t(19) = 0.78$, $p = 0.44$, Cohen's $d = -0.17$; Competition, $t(19) = 0.001$, $p = 1$, Cohen's $d = 0$; **Fig. 2B, *right***).

Collectively these results align with suggestions that the left and right FFA perform different computations[29,52-55] by demonstrating that although the left FFA prefers peripheral faces over peripheral objects, it remains sensitive to spatial location, with a stronger preference for faces in the right (contralateral) visual field than the left (ipsilateral) visual field. Face-selectivity in the right FFA, on the other hand, does not exhibit this sensitivity to spatial location. Taken together, the results imply that the left FFA encodes information about the location of faces, relative to fixation, via a coordinate system that capitalises on the contralateral bias; the strongest face-selective response indicates foveal presentation, the weakest face-selective response indicates ipsilateral presentation.
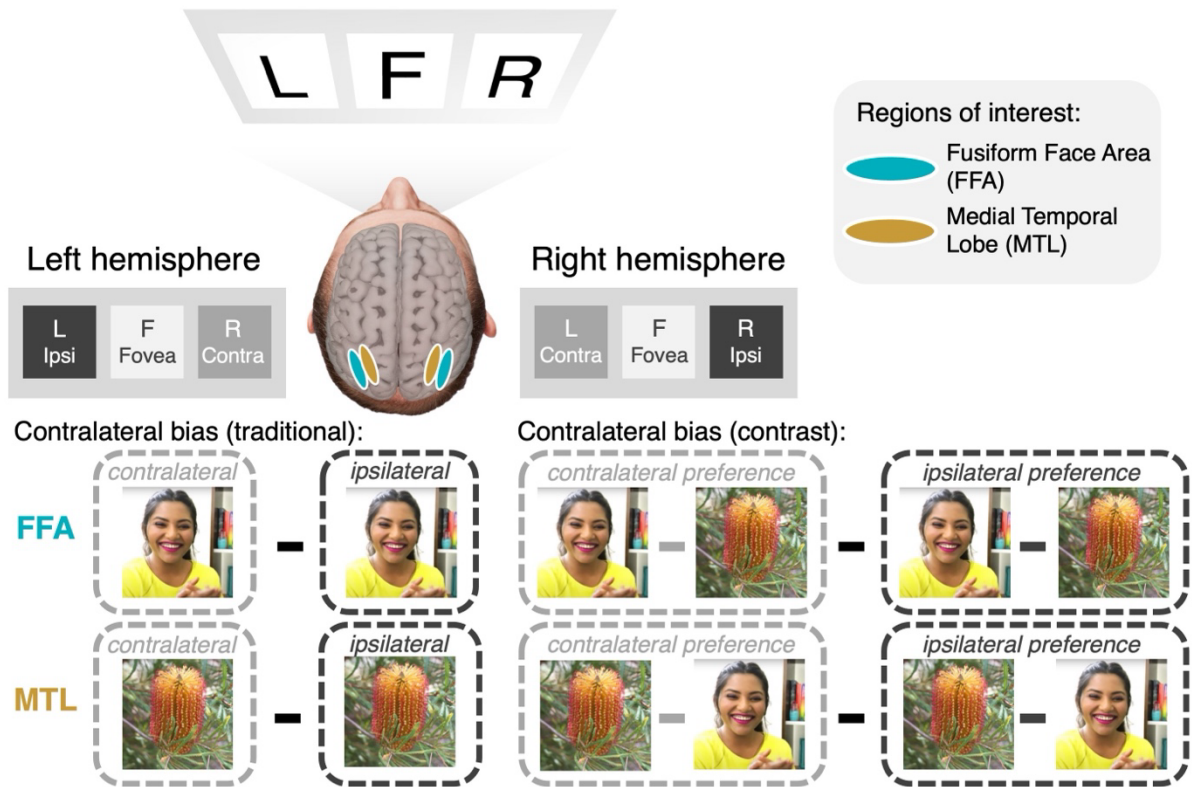
Next, we assessed neural activity in the MTL. To quantify sensitivity to the preferred stimulus category (objects) in the MTL, we computed *d'* scores for each ROI, and each participant, using the following formula:

$$d' = \frac{[\bar{\beta}objects - \bar{\beta}faces]}{\sqrt{[\sigma^2objects + \sigma^2faces]}\frac{1}{2}}$$
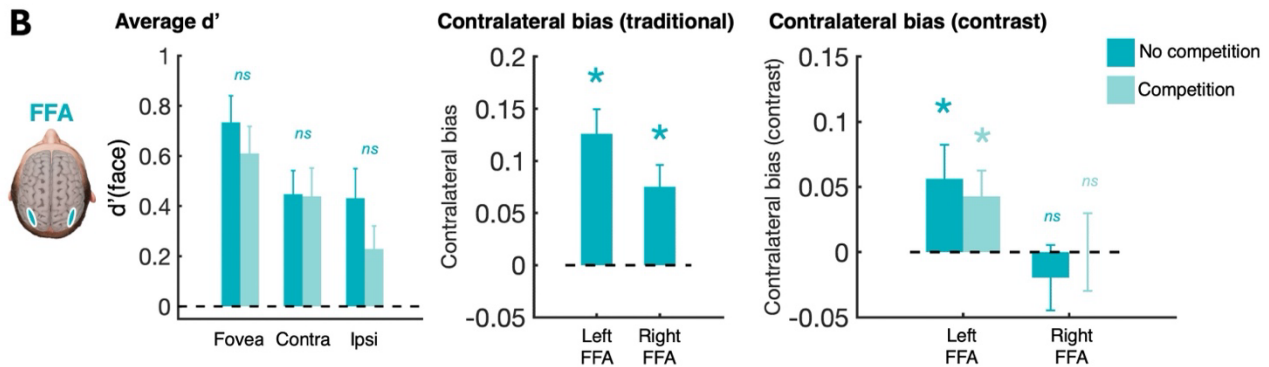
When we performed the same analyses for the MTL as were described above for the FFA, several key differences emerged between these two category-selective regions. For example, while competitive inputs did not reduce the FFA's preference for faces, competitive inputs reduced the MTL's preference for objects in every screen location (paired *t*-tests, two-tailed, foveal presentation, $t(39) = 2.48$, $p = 0.02$, Cohen's $d = 0.39$; contralateral presentation, $t(39) = 8.0$, $p < 0.001$, Cohen's $d = 1.27$; ipsilateral presentation, $t(39) = 3.81$, $p < 0.001$, Cohen's $d = 0.6$; **Fig. 2C, *left***). Indeed, for the MTL, competitive inputs eliminated the preference for objects in the ipsilateral visual field (one sample *t*-tests, almost all *p*-values < 0.001, Cohen's d values ranged from $2.4 - 0.57$; the only exception was the *p*-value associated with ipsilateral presentation in the Competition condition, $t(39) = 0.89$, $p = 0.381$, Cohen's $d = 0.14$; **Fig. 2C, *left***). These results suggest that the stimulus category preference for faces in the FFA is more robust to competitive inputs than the stimulus category preference for objects in the MTL.

Similarly, although the left and right MTL showed the expected contralateral bias when using the traditional calculation (one sample t-tests, two-tailed; left MTL, $t(19) = 8.85$, $p < 0.001$, Cohen's $d = 1.98$; right MTL, $t(19) = 11.01$, $p < 0.001$, Cohen's $d = 2.46$; **Fig. 2C, *middle***), when contralateral bias was calculated as a function of the contrast between faces and objects, the right MTL had a preference for objects over faces that was stronger in the left (contralateral) visual field than the right (ipsilateral) visual field (one sample t-tests, two-tailed; No Competition, $t(19) = 5.73$, $p < 0.001$, Cohen's $d = 1.28$; Competition, $t(19) = 3.27$, $p = 0.002$, Cohen's $d = 0.73$; **Fig. 2C, *right***). This was also true of the left MTL when there were no competitive inputs present (one sample t-tests, two-tailed; No Competition, $t(19) = 2.36$, $p = 0.03$, Cohen's $d = 0.53$; Competition, $t(19) = 0.167$, $p = 0.87$, Cohen's $d = 0.04$; **Fig. 2C, *right***). Therefore, the differences between the FFA (**Fig. 2B, *right***) and the adjacent MTL (**Fig. 2C, *right***) highlight a potential increase in lateralised function within the face-selective network.
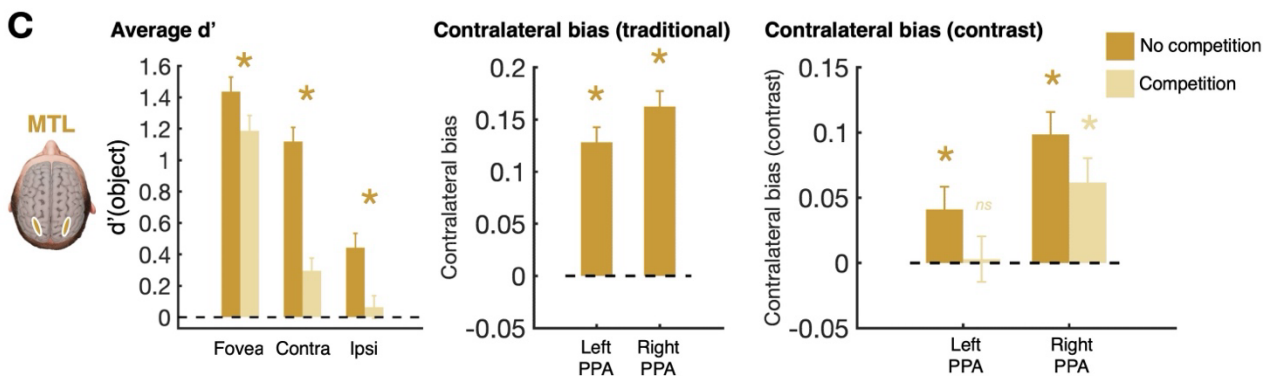
Fig. 2. Preference for faces in the FFA survives competition from peripheral stimuli. (A). *Top,* schematic illustrating how left (L), foveal (F) and right (R) visual fields were converted to contralateral (Contra), foveal (Fovea) and ipsilateral (Ipsi) visual fields for each hemisphere. *Bottom,* visual representation of the formula used to compute contralateral biases in the FFA and MTL. *Bottom left,* traditionally contralateral biases reflect the response to the preferred stimulus in the ipsilateral visual field subtracted from the response to the preferred stimulus in the contralateral visual field. *Bottom right,* in this study we measured contralateral biases as function of the preference for faces over objects (FFA) or objects over faces (MTL). **(B).** Results for the FFA visualised as bar graphs (for all three plots, error bars = +/- standard error). *Left,* asterisks flag significant comparisons between the No Competition and Competition conditions. *Middle and right,* asterisks

10

1   flag contralateral biases greater than zero. **(C).** Results for the MTL visualised as bar graphs (for all three plots, error bars

2   = +/- standard error). *Left,* asterisks flag significant comparisons between the No Competition and Competition conditions.

3   *Middle and right,* asterisks flag contralateral biases greater than zero.

FFA shows a stronger category bias with competitive inputs

For each participant, we directly compared spatial and category biases in the left and right FFA by creating two bias scores for every voxel (see below).

$$spatial\ bias = |[\beta_{left\ faces} + \beta_{left\ objects} \div 2] - [\beta_{right\ faces} + \beta_{right\ objects} \div 2]|$$

$$category\ bias = |[\beta_{left\ faces} + \beta_{right\ faces} \div 2] - [\beta_{left\ objects} + \beta_{right\ objects} \div 2]|$$

We created an index score by subtracting each voxel's category bias from its spatial bias such that a positive index score indicated that the voxel had a spatial bias that was greater in magnitude than its category bias. Conversely, a negative index score indicated that the voxel had a category bias that was greater in magnitude than its spatial bias. A similar approach was previously used by Silson et al.[27] who observed a transition from stronger spatial biases in the early visual cortex to stronger category biases in the anterior portion of the FFA[27]. Across individual participants, the proportion of FFA voxels with a stronger category bias (i.e., a negative bias) than a spatial bias (i.e., a positive bias) is plotted in **Figure 3A** (*left,* when competitive inputs were not present; *right,* when competitive inputs were present). The right FFA had a higher proportion of category-biased voxels than the left FFA (Wilcoxon signed rank tests for paired samples, two-tailed; No Competition, $z = 3.14$, $p = 0.002$; Competition, $z = 3.77$, $p < 0.001$). Interestingly, while there was no evidence that the proportion of category-biased voxels in the left FFA differed between the no competition condition and the competition condition (Wilcoxon signed rank test for paired samples, two-tailed, $z = 0.48$, $p = 0.63$; **Fig. 3B**), the proportion of category-biased voxels in the right FFA *increased* when competitive inputs were introduced (Wilcoxon signed rank test for paired samples, two-tailed, $z = 2.63$, $p = 0.008$; **Fig. 3B**).

In addition, we performed group-level paired t-tests in the brain volume to compare spatial bias scores and category bias scores. Two tests were performed: the first was based on data from the No Competition condition, and the second on data from the Competition condition (see STAR methods). These tests revealed a cluster of voxels in the anterior portion of the right FFA that encoded category preferences more strongly than spatial preferences, regardless of whether competitive inputs were present or not (see **Fig. 3A** for beta maps). To investigate this further we plotted the *t*-values for every FFA voxel as a function of its anterior-posterior (A-P) location (**Fig. 3C**). Consistent with the results of Silson et al.[27], when there were no competitive inputs, we found correlations between *t*-values and A-P location present suggesting that the anterior pole of the FFA was more biased towards stimulus category than stimulus location (left FFA, $N = 172$, Spearman's $\rho = 0.67$, $p < 0.001$; right FFA, $N = 318$, Spearman's $\rho = 0.61$, $p < 0.001$, two-tailed; **Fig. 3C**). However, in both hemispheres these correlations were eliminated by the introduction of competitive inputs (left FFA, $N = 172$, Spearman's $\rho = 0.04$, $p = 0.56$; right FFA, $N = 318$, Spearman's $\rho = 0.09$, $p = 0.1$, two-tailed; **Fig. 3C**). The proportion of category-biased voxels in the right FFA increased from 50.1% in the no competition condition to 88% in the competition condition (two-proportion *z-*

test, $z = 10.16$, $p < 0.001$). By contrast, the proportion of category-biased voxels in the left FFA increased from only 32.6% in the no competition condition to 48.8% in the competition condition (two-proportion z-test, $z = 3.07$, $p = 0.002$). In sum, in the absence of competitive inputs, our findings are consistent with those of Silson et al.[27]; specifically, activity in the anterior pole of the left and right FFA was more biased by stimulus category than stimulus location When competitive inputs were present, however, an increased number of voxels in the right FFA were more biased by stimulus category than stimulus location. There was no evidence that these voxels were clustered together in the anterior portion of the FFA.

Overall, the results shown in **Figure 3** indicate that the right FFA has a higher proportion of voxels with a stronger category bias than a spatial bias. This proportion increased with the introduction of competitive inputs, suggesting perhaps that more resources are assigned or engaged under noisier (more naturalistic) conditions. These results align with those in **Figure 2B**, which implied that sensitivity to peripheral face stimuli in the right FFA were similar irrespective of whether stimuli were presented in the contralateral or ipsilateral visual field. Whereas the left FFA showed a contralateral bias, here we find that more left FFA voxels are biased by stimulus location than stimulus category. These findings suggest that the left FFA contributes differently to the rapid detection of peripheral faces than the right FFA. It is clear, however, that the right FFA is biased toward peripheral face stimuli and that this preference is robust to competitive inputs.
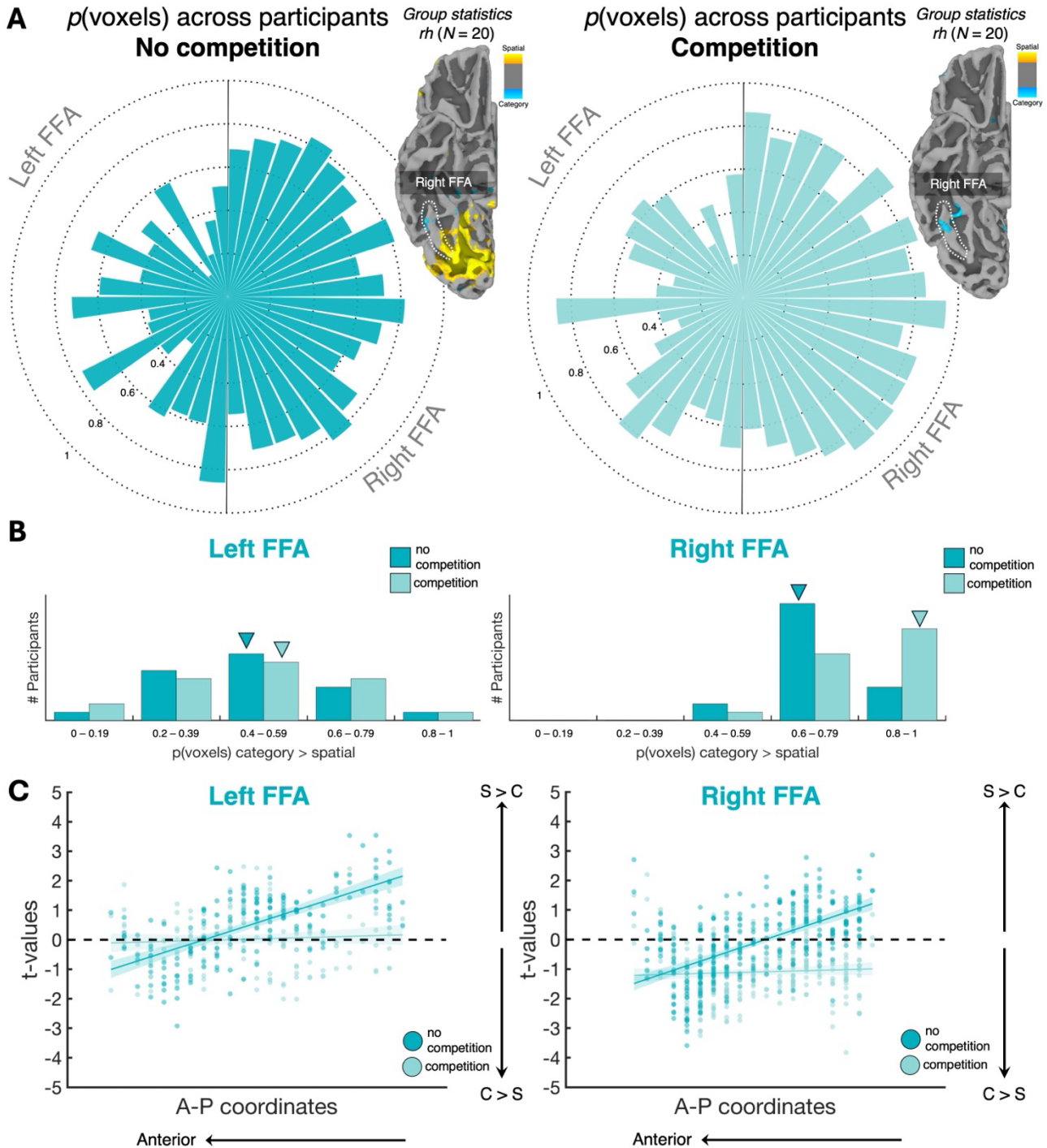
Fig. 3. Directly comparing category biases and spatial biases in the FFA. (A). Radial plots showing the proportion of category-biased FFA voxels for each participant (*N* = 20). *Left,* based on data from the no competition condition with each wedge representing the data from one participant. *Right,* based on data from the competition condition with each wedge representing the data from one participant. Floating above both radial plots is the whole brain data associated with the index values averaged across all 20 participants (right hemisphere only). The data have a statistical threshold of *p* = 0.05 (uncorrected). Yellow voxels have a spatial bias that is greater in magnitude than its category bias. Blue voxels have a category bias that is greater in magnitude than its spatial bias. **(B).** The distribution of category-biased FFA voxels across the sample. *Left,* based on data from the left FFA and, *right,* based on data from the right FFA. Arrows indicate median scores for the No Competition (dark teal) and Competition conditions (light teal). **(C).** Scatterplots visualizing the

1   relationship between t-values (i.e., from the contrast between spatial bias scores and category bias scores) and A-P

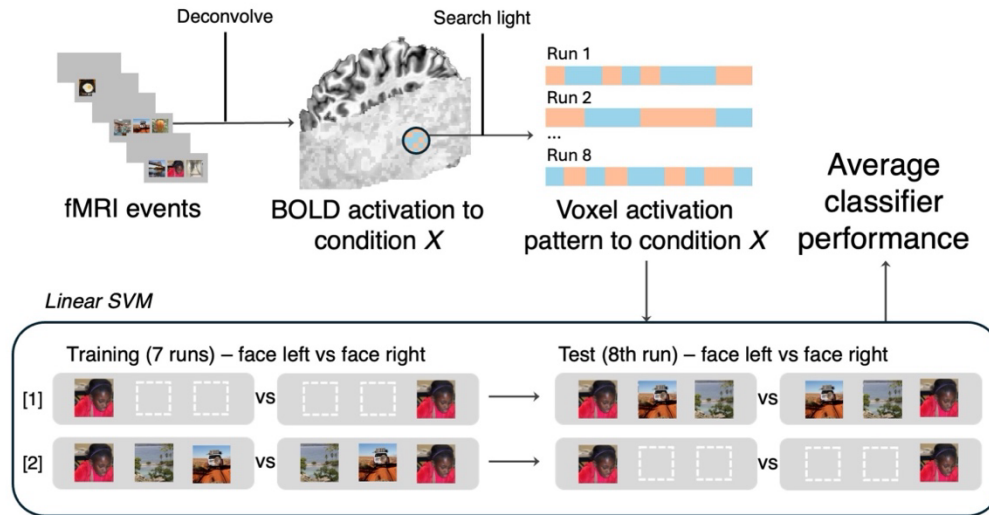2   coordinates in the left FFA (on the left) and the right FFA (on the right).

3

4

The left Fusiform Face Area encodes the spatial location of peripheral faces

Taubert et al.[13] used a searchlight decoding analysis to reveal that the location of a face stimulus was encoded by patterns of activity across face-selective voxels in the macaque visual cortex. Following from that work, we used a cross-decoding leave-one-run-out searchlight analysis to identify regions that distinguished the peripheral locations of face stimuli (left or right visual field), irrespective of whether competitive inputs were present or not (see **Fig. 4A** and STAR methods for more details). This analysis was performed separately for each participant, with average decoding performance projected onto a partially inflated cortical surface (see **Figure 4B**). This analysis identified 8 clusters at the group level (minimum cluster threshold = 10 voxels) with decoding accuracy greater than 65% (chance = 50%; see **Table 1**). The first was a region in the left lateral occipital cortex, which approximates the location of the left Occipital Face Area (OFA) (**Fig. 4B**). The second was a region within the left FFA (**Fig. 4B**). Additionally, this analysis identified the intraparietal cortex, left visual area 3 and left area 9 in prefrontal cortex (for a full list see **Table 1**).

The intraparietal cortex is thought to play a role in driving eye movements toward arousing stimuli via direct projections to oculomotor centers[56]. . Inactivation of face-selective regions in the macaque ventral visual cortex changes the response profile of the intraparietal sulcus[57], suggesting a causal relationship, and this region is also engaged in the allocation of attention to peripheral visual targets[58-60]. The intraparietal sulcus thus belongs within a network responsible for the detection and prioritisation of faces. Interestingly, there is evidence that Visual Area 3 (V3), especially in the left hemisphere, is selective for stimuli with a high curvature index[37]. In the macaque model, researchers have posited that "curvature patches" are at least partially responsible for the rapid discrimination of animate and inanimate objects[61]. Area 9 in the prefrontal cortex has been implicated in regulating social judgements and in making sense of others[62,63]. In other words, many of the regions identified by the searchlight decoding analysis contribute to behaviour in ways that would promote the detection, localisation, and rapid evaluation of social agents.

In sum, the decoding results indicate that the OFA and the left FFA in the ventral visual cortex encode the location of peripheral faces (left vs right visual field) and that this code generalises from no competition conditions to competition conditions and vice versa. Similarly to the results of Taubert et al.[13], these findings imply that the primate visual cortex encodes information about the spatial location of faces in the larger visual field. However, unlike in the macaque, this function appears to be restricted to distinct, posterior nodes of the face-selective network in humans – specifically, the OFA and posterior pole of the left FFA (**Fig. 4**). Importantly, the results of the searchlight analysis are consistent with the results presented in **Figure 2B**; the left FFA has a strong contralateral bias which may afford this region the capacity to encode whether a peripheral face is positioned in the left or right visual field. Surprisingly, we found no evidence that this capacity is shared by the right FFA.
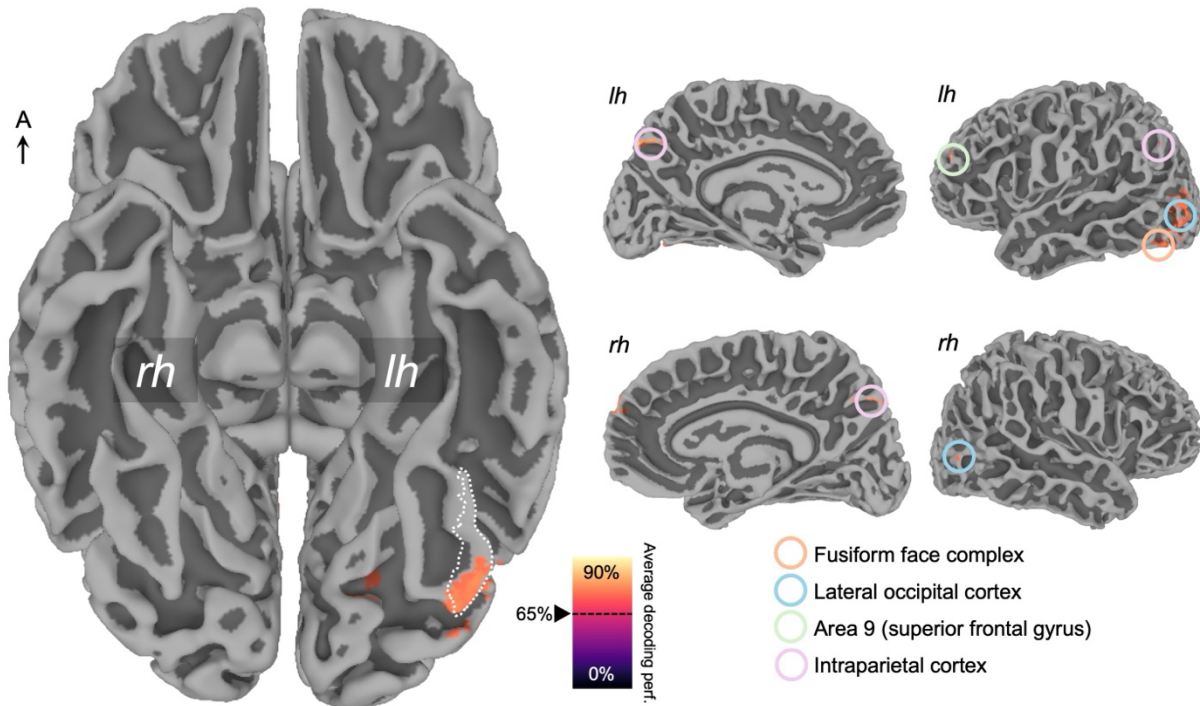
1

2 **Fig. 4. fMRI cross-decoding searchlight results. (A).** Schematic of the leave-one-run-out cross-validation approach to
3 the whole-brain decoding searchlight analysis. The classifier was [1] trained on data from the No Competition condition
4 and tested on data from the Competition condition, and [2] trained on data from the Competition condition and tested on
5 data from the No Competition condition. Results for these two cross-decoding conditions were averaged **(B).** The
6 searchlight analysis was conducted for each participant; we then averaged all 20 decoding maps. Locations of greatest
7 decoding accuracy (i.e., greater than 65%) were projected onto a partially inflated MNI cortical surface. On the left is the
8 ventral surface, on the right are the lateral and medial views of the left hemisphere (top) and the right hemisphere (bottom).
9 One of the locations visible on the ventral surface overlaps with the FFA in the left hemisphere. For illustration, the boundary
10 of the left FFA mask has been marked on the ventral surface with a white dashed line (left panel). All regions comprised of
11 40 voxels (or more) identified by the searchlight decoding analysis in the volume are listed in **Table 1**.

1 **Table 1.** MNI coordinates for regions identified by searchlight decoding analysis (average
2 performance greater than 65%; all regions comprised of 40+ voxels).

Number of voxels	x	y	z	Label (MNI Glasser HCP Atlas)
640	-44.6	-82.8	1.4	Left lateral occipital cortex
224	-41.1	-77.5	-16.1	Left fusiform face complex
105	-0.9	-75.8	48.6	Precuneus
99	-25.4	64.2	13.6	Left area 9
80	-48.1	-54.8	43.4	Left intraparietal cortex (IPS and IPL)
59	-20.1	-72.2	-9.1	Left third visual area (V3)
49	-42.9	53.8	18.9	Left area 9 - 46v
40	51.6	-74	8.4	Right lateral occipital cortex

3

Discussion

In this study, our primary goal was to determine whether the human Fusiform Face Area (FFA) contributes to the rapid detection of peripheral faces. Specifically, whether its category selectivity for faces persists when stimuli are presented in the periphery and under conditions of visual competition from adjacent inputs. To address this, we first validated a set of highly variable, naturalistic images using a behavioural similarity judgement task, ensuring that our faces, objects, and scenes were perceived as distinct categories despite uncontrolled low-level differences. We then used ultra-fast 7-T fMRI to measure neural responses to these stimuli while systematically varying stimulus position (foveal, left, right) and the presence or absence of competing inputs. This factorial design enabled us to disentangle the influence of spatial location and competition on the category selectivity of the FFA, and a neighbouring object-selective area (MTL). The combination of naturalistic stimuli, behavioural validation, and ultra-fast neuroimaging allowed us to test the response profile of the FFA under conditions that more closely approximate real-world vision, while maintaining the experimental control necessary for unambiguous interpretation.

As expected, we confirmed that the FFA has a traditional spatial bias, with stronger responses to face stimuli presented in the contralateral then the ipsilateral visual field. This was also true of the object-selective MTL, which showed stronger responses to object stimuli presented in the contralateral visual field. Additionally, we discovered that the FFA has a strong preference for face stimuli that is tolerant of competitive inputs. This implies that the FFA is equipped to detect and process peripheral faces, distinguishing them from peripheral objects, even when participants are viewing more cluttered visual arrays. However, unlike the FFA, the MTL had a preference for object stimuli that was reduced by the introduction competitive inputs. Collectively, these findings provide empirical support for the idea that the face-selective cortical network contributes to the rapid detection and prioritization of face stimuli[22-24,64,65]. Further, these findings also highlight the strength of the inferences that can be drawn from experiments that measure the responses of the visual system under more naturalistic circumstances, without abandoning experimental control[44,66,67].

When we probed the interaction between the biases towards contralateral space and face stimuli, we found evidence of functional lateralisation associated with the FFA complex[29,52-55]; the left FFA had a preference for faces over objects that was larger on the contralateral visual field than the ipsilateral visual field, whereas this was not the case for the right FFA. The results in **Figure 2B**, together with the whole-brain analysis in **Figure 4**, suggest that there could be a specific role for the left FFA in face detection. A recent laminar fMRI study reported that face-selective responses in the FFA are likely fed to primary visual cortex (V1)[68]. Moreover, there is evidence that peripheral visual targets are represented in primary visual cortex as if they appear in a foveal location[60,69]. If peripheral faces can be considered "automatic" targets, owing to their social or evolutionary significance, then any peripheral face might be foveally represented in V1. Further, this remapping might be accomplished via feedback from the left FFA to V1. Interestingly, the remapping of peripheral targets to foveal resources is also thought to mediated by activity in the intraparietal cortex[60], a region

19

identified by the searchlight decoding analysis in the current study. In sum, it seems possible that information about the location of faces is fed back from the FFA into structures responsible for redirecting attention to peripheral visual targets. However, this idea requires further investigation.

When we compared biases directly, we found that the right FFA had a stronger bias towards stimulus category than stimulus location. This is consistent with the observed lack of a face-selective contralateral bias in **Figure 2B** and suggests that the right FFA responds more to faces and objects regardless of where stimuli are presented in the visual field. Surprisingly, this category bias only increased when competitive inputs were introduced. Notably, evidence of this robust preference for face stimuli was absent in the macaque model[13] and, as such, this functionality of the right FFA may represent a more recent evolutionary refinement of a pre-existing repertoire. It has been argued that the face-selective network in humans is likely to be a composite system, comprised of both ancestral (i.e., old) and derived (i.e., new) structures and functions[70]. Additionally, there has been speculation that the contribution of the right FFA to behaviour could be unique to the human lineage[71-73]. Evidence for this discontinuity is suggested by the absence of the fusiform gyrus at a structural level in the macaque brain, as well as a dearth of evidence consistent with hemispheric lateralisation within the macaque face-selective network[71]. This raises the question, what *is* the unique contribution of the right FFA to human behaviour?

The robust preference for faces over objects, irrespective of spatial location or the presence of competitive inputs, implies that the right FFA is an important hub within the face detection and recognition system. Previous neuropsychological studies have linked the right FFA to the recognition of faces at the sub-ordinate level (i.e., face identification[74-76] It follows that the current findings might indicate that the right FFA is engaged, and that the processes underlying individual face recognition begin prior to fixation. It is also possible that the right FFA plays a broader role in the social evaluation of faces, related to the assessment of familiarity[77] or approachability[78], which would explain evidence for a direct connection between the fusiform gyrus and the amygdala[79-82]. In this schema, it also seems likely that the left and right FFA work together to determine the spatial location of a face (left FFA) and then begin to evaluate that face (right FFA) to inform social behaviours, such as whether to approach or avoid a detected social agent.

While face detection has been widely presumed to be the first foundational step towards more complex computations such as individual face recognition[17,26,83], it has received very little attention from researchers in the field of cognitive neuroscience. Indeed, theories of face detection, and how it is accomplished, have relied on advances in computer modelling and the development of *in silico* face detection algorithms[83]. But these algorithms are known to make routine mistakes that our *in vivo* face detection system does not. For example, multiple studies have demonstrated that face detection algorithms are often biased towards the faces of Caucasian males arising from the sociotechnical contexts of innovation, design and production[84-86]. This demonstrates that *in silico* face detection systems are vulnerable to training effects – in other words, they are calibrated to the type of faces to which they have been exposed. In contrast, there is evidence that our *in vivo* face

detection system is operational from birth (i.e., prior to any relevant visual experience)[22,24,26,87]. This distinction between *in vivo* and *in silico* face detection is further illustrated by the failure of machines to detect objects that look like faces, i.e., the face pareidolia illusion. While adult humans, infants and other primates can detect examples of face pareidolia as if they were real faces[23,46,88-93], only deep neural nets trained with a broad range of animal faces[94], or trained to perform face recognition in parallel to object recognition[95], have accurately classified novel examples of face pareidolia as being faces. Indeed, from birth and throughout life humans appear to remain broadly tuned to a diverse range of faces and face-like patterns, irrespective of increases in exposure or changes in visual diet[87]. It follows that, at this stage, *in vivo* face detection is functionally distinct from *in silico* face detection. Thus, when the goal is to understand how we detect faces across the visual field, it is vital that we design experiments to better understand how face detection is accomplished by the human brain.

STAR Methods

Key resources table

REAGENT or RESOURCE	SOURCE	IDENTIFIER
Software and algorithms		
jspsych	https://www.jspsych.org/latest/	RRID:SCR_023508
Matlab_R2023b	https://au.mathworks.com/	RRID:SCR_001622
Psychophysics Toolbox	http://psychtoolbox.org/	RRID:SCR_002881
AFNI	https://afni.nimh.nih.gov/	RRID:SCR_005927

Participants

Seventy-five participants initially volunteered to participate in the behavioural experiment, but only the data from the 73 who completed all 300 trials were included in the analysis (43 females, Mage = 20, SD_{age} = 2.25). All participants had normal or corrected to normal vision and gave written informed consent prior to data collection. All procedures for the behavioural experiment were approved by The University of Queensland Human Research Ethics Committee (2021/HE002275).

A total of 21 participants volunteered to participate in the fMRI experiment. One participant's data were removed from the analysis because the key regions of interest (i.e., the FFA and the MTL) could not be identified in either hemisphere. Therefore, the final sample consisted of 20 adults (13 females, Mage = 26.8 years, SD_{age} = 6.8; 18 had a right-hand preference on the Flinders Handedness survey[96]). All participants had normal or corrected to normal vision and gave written informed consent prior to data collection. All participants completed the localiser and main experiment across two separate sessions. All procedures for the fMRI experiment were approved by The University of Queensland Human Research Ethics Committee (2020/HE003101).

Overview of the experimental design

The behavioural experiment was conducted first to validate the stimulus set. The 180 wild-type stimuli were sorted into three conditions (faces, objects and scenes) based on: (1) the presence of a face, (2) the presence of a centrally positioned object or (3) the presence of a horizon. However, given the level of heterogeneity among the 180 stimuli, it was important to confirm that the stimuli assigned to a given condition were perceived as being more similar to each other than to the stimuli assigned to the other conditions. Therefore, we collected triplet odd-one-out data and performed a Representational SimilarityAnalysis[49,97].

With the stimulus selection validated we built the Functional Localiser and the Competition Task for the scanner. Every participant recruited for the fMRI experiment completed two

experimental sessions on separate days. Experiment sessions were scheduled at the same time of day and were at least 3 days apart. All Functional Localiser runs were completed in the first session (2-3 runs per participant). The 8 runs associated with the Competition Experiment were completed in the second session.

7.0T ultra-fast scanning parameters

All functional data were acquired on a 7.0 T Siemens Magnetom MRI scanner at the Centre for Advanced Imaging at The University of Queensland (St Lucia, QLD, Australia). Partial volumes positioned and optimised for the collection of BOLD data from temporal cortex were acquired using a single transmit coil and a 32-channel receive nova medical head coil (32 slices; 1.8mm isotropic; TR, 500 ms; TE, 25.20 ms; FOV, 209 mm; flip angle, 40°). T1-weighted anatomical images were acquired in both sessions using the magnetization prepared 2 rapid gradient echo (MP2RAGE) sequence (256 slices; 0.8 mm isotropic; TR, 4.3 s; TE, 2.45 ms; TI, 840 ms; flip angle, 5°).

Visual stimuli and tasks

Behavioural Experiment. Forty-five naturalistic faces were sourced from online depositories associated with two previous studies[40,88]. Forty-five object-centered scenes were sourced from online depositories associated with two previous studies[88,98]. The 90 scene-oriented scenes comprised 45 indoor scenes and 45 outdoor scenes taken from the SUN database[99] together with photographs taken from the private library of one of the authors (JT). Each stimulus was resized to 400 x 400 pixels but was otherwise unaltered. In this experiment, participants rated the similarity between the 180 experimental stimuli using a triplet odd-one-out task[46,49,100]. The experiment was programmed in jsPsych[101] and hosted on Pavlovia[102]. On each trial, three experimental stimuli were presented simultaneously, and participants were asked to choose the odd one out by clicking on the stimulus (**Fig. 1B**). Stimuli were presented equidistant from fixation in a triangle pattern. There were 300 trials in the experiment.

All trials from all participants were collated and the behavioral responses were used to construct a representational dissimilarity matrix (RDM). For each trial, dissimilarity was calculated for the pairs of stimuli (3 separate pairs for the 3 distinct stimuli). The stimulus chosen as the odd-one-out was coded as dissimilar from each of the other two stimuli (values of 1), and the two other stimuli were coded as similar (value of 0). The dissimilarity of each stimulus pair (e.g., face #1 vs object #5) was calculated as the mean dissimilarity value for all trials in which those two stimuli were presented together. These mean values were used to construct a 180 x 180 RDM (**Fig. 1C**). For visualization, we applied multidimensional scaling (MDS) to the resulting matrix and plotted the first two dimensions (**Fig. 1D**). This plot shows all 180 stimuli, with closer proximity between any two stimuli representing greater perceived similarity.

Functional Localiser. We ran an independent localiser to identity the left and right FFA, as well as the left and right MTL. To this end, we employed the stimuli taken from the fLoc task[103] (retrieved from http://vpnl.stanford.edu/fLoc/); we used the 44 faces, 44 objects, 44 characters, and 44 noise images (400 x 400 pixels in size). These stimuli were presented in a rapid event-related design, with each stimulus shown for 200 ms and replaced with a blank screen for 300 ms. Each stimulus was presented four times per run and trial order was determined at random. Participants lay supine in the scanner and viewed the stimuli via rear projection onto a mirror mounted on the head coil. The stimuli subtended 5 x 5 DVA and were presented behind a central fixation point. Participants were asked to focus on the central fixation point for the length of each run and to press a button when a stimulus was tilted 6 degrees to the left or to the right. There were 32 tilted images per run. Each run began with an initial fixation period of 2 seconds. Thus, we collected 708 volumes of data per localiser run. Participants completed 2 – 3 localiser runs in a session separate from the Competition Experiment.

Competition Experiment. The 180 experiment stimuli from the Behavioural Experiment were used in the Competition Experiment. Within a run, every face stimulus was presented once in each of the 6 "face" conditions (**Fig. 1E**), and every object was presented once in each of the 6 "object" conditions. Therefore, there were 540 unique trials per run. This design was made feasible through the implementation of the ultra-fast EPI sequence with a TR of 500 ms.

Using the same apparatus and rapid event-related design as the localiser experiment, stimuli were presented in one of three screen locations (left [the centre of stimuli were positioned 7 degrees to the left of the centre of the screen], right [the centre of stimuli were positioned 7 degrees to the right of the centre of the screen], fovea [the centre of stimuli were positioned at the centre of the screen]). The stimuli were presented at the same physical size (equivalent to 5 x 5 degrees of visual angle when presented at the foveal). To present stimuli in all three locations, we utilised the full length of the projection-to-mirror set up in the scanner and, for that reason, it was necessary to verify that every participant could see stimuli in all three screens positions before any data were collected. When an experimental run was initiated, every face and object stimulus was randomly paired with two scene stimuli for the purpose of competition trials. Thus, within a run, a face was seen with the same two scene stimuli exactly 3 times (i.e., once when the face was presented to the left visual, once when then face was presented to the right visual field, and once when the face was presented to the fovea).

The task for participants was to focus on the central fixation dot comprised of three black and white concentric circles. The contrast of these circles reversed 24 times per run. When a reversal occurred, the participants were instructed to press a button and this had to occur within 500 ms of the event to be reported as correct. Averaged across participants and runs, mean accuracy in the fixation task was 93.6% (SD = 2.8%). The beginning of each run began with 2 seconds of fixation. Subsequently, the unique trials were presented in random order with stimuli on for 200 ms and off

1 for 300 ms. In total we collected 544 volumes of data per run and 4352 volumes of data per
2 participant (i.e., 8 runs).
3

fMRI data processing

5 Data from the Functional Localiser and Competition Experiments were analyzed using AFNI[104,105]
6 and visualised using SUMA[106]. We used the AFNI SSwarper program[107] to skull strip each
7 participant's T1 scans and to calculate the nonlinear warp to the MNI152 template[108-110].

8   After moving the functional data into the MNI152 common space, we employed afni_proc.py
9 tools to build the fMRI processing pipeline[111]. To begin, the first four volumes at the beginning of
10 every run were discarded. The remaining volumes were slice-time corrected, realigned to the first
11 volume of each session, and spatially smoothed with a 3 mm FWHM Gaussian kernel. Signal
12 intensity was normalized to the mean signal value within each run and multiplied by 100 so that the
13 results after analysis represented percentage signal change from mean. Volumes associated with
14 motion greater than 1 mm were censored; using this stringent criterion, there were three participants
15 with 1 volume of data above the motion limit. We used the 3dToutcount function to flag any voxels
16 in a volume of data with a signal intensity greater than 3 standard deviations from other voxels in the
17 brain mask. Our acceptable outlier fraction was set at 0.1. Using this stringent criterion $0 - 18$
18 volumes were censored per participant. Regressors of interest were created by convolving each of
19 the 4 conditions (in the Functional Localiser) or 12 conditions (in the Competition Experiment) with
20 the haemodynamic response function and then input into a general linear model (GLM) for parameter
21 estimation. Additionally, the slow drifts and six head movement parameters (roll, pitch, yaw, dS, dL,
22 dP) were included in the GLM as regressors of no interest.
23

24 *ROI definition.* The fMRI data from the Functional Localiser sessions were averaged across all 20
25 participants. At the group level, we defined the FFA and MTL, bilaterally, using the following
26 contrasts:
27

28 $$Face-selective = \left(3 \times \overline{\beta_{faces}}\right) - \overline{\beta_{objects}} - \overline{\beta_{noise\ images}} - \overline{\beta_{characters}}$$
29 $$Object-selective = \left(3 \times \overline{\beta_{objects}}\right) - \overline{\beta_{faces}} - \overline{\beta_{noise\ images}} - \overline{\beta_{characters}}.$$
30

31 The FFA masks were created using the face-selective contrast in combination with a statistical
32 threshold of $p = 0.001$ (uncorrected) and a cluster threshold of 10 voxels (NN2). The right FFA was
33 a cluster identified in the right fusiform gyrus (*MNI coordinates,* +44.3 -55.3 -21.8; *size,* 318 voxels).
34 The left FFA was a cluster identified in the left fusiform gyrus (*MNI coordinates,* -44.4 -58.3 -22; *size,*
35 172 voxels). The MTL masks were created using the object-selective contrast in combination with a
36 statistical threshold of $p = 0.001$ (uncorrected) and a cluster threshold of 10 voxels (NN2). The right
37 MTL was a cluster identified in the right posterior medial temporal lobe (*MNI coordinates,* +27.7 -
38 48.1 -10.2; *size,* 381 voxels). The left MTL was a cluster identified in the left posterior medial temporal

lobe (*MNI coordinates,* -21.1 -49.6 -9.4; *size,* 306 voxels). These four masks, which were based on the average group response in the Functional localiser, were then used to mask the Competition Experiment data for each individual participant. Therefore, for every participant, we analysed an equal number of voxels per ROI.

Searchlight decoding analysis. The decoding searchlight was conducted using the Newton linear SVM classifier implemented in TDT[112], with a searchlight radius of 3 voxels. We used a leave-one-run-out cross-validation approach. The searchlight was conducted in each participant's native brain space, and the results of the group were averaged together and visualized (see **Figure 4**).

Author contributions

J.T., A.K.R. created the stimuli. J.T. and A.K.R. conducted the experiments. J.T. analysed the results. J.T., A.K.R. and J.B.M. interpreted the results. J.T., A.K.R. and J.B.M. wrote the manuscript.

Declaration of interests

The authors declare no competing interest

References

1. Dumoulin, S.O., and Wandell, B.A. (2008). Population receptive field estimates in human visual cortex. NeuroImage *39*, 647-660. https://doi.org/10.1016/j.neuroimage.2007.09.034.

2. Hubel, D.H., and Wiesel, T.N. (1965). RECEPTIVE FIELDS AND FUNCTIONAL ARCHITECTURE IN TWO NONSTRIATE VISUAL AREAS (18 AND 19) OF THE CAT. J Neurophysiol *28*, 229-289. 10.1152/jn.1965.28.2.229.

3. Elul, D., and Levin, N. (2024). The Role of Population Receptive Field Sizes in Higher-Order Visual Dysfunction. Curr Neurol Neurosci Rep *24*, 611-620. 10.1007/s11910-024-01375-6.

4. Verhoef, B.E., Bohon, K.S., and Conway, B.R. (2015). Functional architecture for disparity in macaque inferior temporal cortex and its relationship to the architecture for faces, color, scenes, and visual field. J Neurosci *35*, 6952-6968. 10.1523/jneurosci.5079-14.2015.

5. Arcaro, M.J., Ponce, C.R., and Livingstone, M.S. (2019). The neurons that mistook Stuart's hat for his face. Journal of vision *19*, 259c-259c. 10.1167/19.10.259c.

6. Finzi, D., Gomez, J., Nordt, M., Rezai, A.A., Poltoratski, S., and Grill-Spector, K. (2021). Differential spatial computations in ventral and lateral face-selective regions are scaffolded by structural connections. Nat Commun *12*, 2278. 10.1038/s41467-021-22524-2.

7. Op De Beeck, H., and Vogels, R. (2000). Spatial sensitivity of macaque inferior temporal neurons. J Comp Neurol *426*, 505-518. 10.1002/1096-9861(20001030)426:4<505::aid-cne1>3.0.co;2-m.

8. Levy, I., Hasson, U., Avidan, G., Hendler, T., and Malach, R. (2001). Center-periphery organization of human object areas. Nat Neurosci *4*, 533-539. 10.1038/87490.

9. Malach, R., Levy, I., and Hasson, U. (2002). The topography of high-order human object areas. Trends Cogn Sci *6*, 176-184. 10.1016/s1364-6613(02)01870-3.

10. Hsiao, J.H., and Cottrell, G. (2008). Two fixations suffice in face recognition. Psychol Sci *19*, 998-1006. 10.1111/j.1467-9280.2008.02191.x.

11. Poltoratski, S., Kay, K., Finzi, D., and Grill-Spector, K. (2021). Holistic face recognition is an emergent phenomenon of spatial processing in face-selective regions. Nat Commun *12*, 4745. 10.1038/s41467-021-24806-1.

12. Henriksson, L., Mur, M., and Kriegeskorte, N. (2015). Faciotopy-A face-feature map with face-like topology in the human occipital face area. Cortex; a journal devoted to the study of the nervous system and behavior *72*, 156-167. 10.1016/j.cortex.2015.06.030.

13. Taubert, J., Wardle, S.G., Tardiff, C.T., Patterson, A., Yu, D., and Baker, C.I. (2022). Clutter substantially reduces selectivity for peripheral faces in the macaque brain. J Neurosci *42*, 6739-6750. 10.1523/jneurosci.0232-22.2022.

14. Zoccolan, D., Cox, D.D., and DiCarlo, J.J. (2005). Multiple object response normalization in monkey inferotemporal cortex. The Journal of neuroscience : the official journal of the Society for Neuroscience *25*, 8150-8164. 10.1523/jneurosci.2058-05.2005.

15. Bao, P., and Tsao, D.Y. (2018). Representation of multiple objects in macaque category-selective areas. Nature communications *9*, 1774. 10.1038/s41467-018-04126-7.

16. Reddy, L., and Kanwisher, N. (2007). Category selectivity in the ventral visual pathway confers robustness to clutter and diverted attention. Current biology : CB *17*, 2067-2072. 10.1016/j.cub.2007.10.043.

17. Robertson, D.J., Jenkins, R., and Burton, A.M. (2017). Face detection dissociates from face identification. Visual Cognition *25*, 740-748. 10.1080/13506285.2017.1327465.

18. Hershler, O., and Hochstein, S. (2009). The importance of being expert: top-down attentional control in visual search with photographs. Atten Percept Psychophys *71*, 1478-1486. 10.3758/app.71.7.1478.

19. Keys, R.T., Taubert, J., and Wardle, S.G. (2021). A visual search advantage for illusory faces in objects. Atten Percept Psychophys *83*, 1942-1953. 10.3758/s13414-021-02267-4.

20. Frank, M.C., Amso, D., and Johnson, S.P. (2014). Visual search and attention to faces during early infancy. J Exp Child Psychol *118*, 13-26. 10.1016/j.jecp.2013.08.012.

21. Hershler, O., and Hochstein, S. (2005). At first sight: a high-level pop out effect for faces. Vision Res *45*, 1707-1724. 10.1016/j.visres.2004.12.021.

22. Goren, C.C., Sarty, M., and Wu, P.Y. (1975). Visual following and pattern discrimination of face-like stimuli by newborn infants. Pediatrics *56*, 544-549.

23. Taubert, J., Wardle, S.G., Flessert, M., Leopold, D.A., and Ungerleider, L.G. (2017). Face Pareidolia in the Rhesus Monkey. Curr Biol *27*, 2505-2509.e2502. 10.1016/j.cub.2017.06.075.

24. Reid, V.M., Dunn, K., Young, R.J., Amu, J., Donovan, T., and Reissland, N. (2017). The Human Fetus Preferentially Engages with Face-like Visual Stimuli. Curr Biol *27*, 1825-1828.e1823. 10.1016/j.cub.2017.05.044.

25. Fletcher-Watson, S., Findlay, J.M., Leekam, S.R., and Benson, V. (2008). Rapid detection of person information in a naturalistic scene. Perception *37*, 571-583. 10.1068/p5705.

26. Johnson, M.H. (2005). Subcortical face processing. Nat Rev Neurosci 6, 766-774. 10.1038/nrn1766.

27. Silson, E.H., Groen, I.I.A., and Baker, C.I. (2021). Direct comparison of contralateral bias and face/scene selectivity in human occipitotemporal cortex. Brain Struct Funct. 10.1007/s00429-021-02411-8.

28. Rossion, B., Dricot, L., Devolder, A., Bodart, J.M., Crommelinck, M., De Gelder, B., and Zoontjes, R. (2000). Hemispheric asymmetries for whole-based and part-based face processing in the human fusiform gyrus. J Cogn Neurosci *12*, 793-802. 10.1162/089892900562606.

29. Meng, M., Cherian, T., Singal, G., and Sinha, P. (2012). Lateralization of face processing in the human brain. Proceedings. Biological sciences / The Royal Society *279*, 2052-2061. 10.1098/rspb.2011.1784.

30. Robinson, A.K., Grootswagers, T., Shatek, S.M., Behrmann, M., and Carlson, T.A. (2025). Dynamics of visual object coding within and across the hemispheres: Objects in the periphery. Sci Adv *11*, eadq0889. 10.1126/sciadv.adq0889.

31. Taubert, J., Apthorp, D., Aagten-Murphy, D., and Alais, D. (2011). The role of holistic processing in face perception: evidence from the face inversion effect. Vision Res *51*, 1273-1278. 10.1016/j.visres.2011.04.002.

32. Taubert, J., Alais, D., and Burr, D. (2016). Different coding strategies for the perception of stable and changeable facial attributes. Sci Rep 6, 32239. 10.1038/srep32239.

33. Yue, X., Cassidy, B.S., Devaney, K.J., Holt, D.J., and Tootell, R.B. (2011). Lower-level stimulus features strongly influence responses in the fusiform face area. Cereb Cortex *21*, 35-47. 10.1093/cercor/bhq050.

34. Taubert, J. (2009). Chimpanzee faces are 'special' to humans. Perception *38*, 343-356. 10.1068/p6254.

35. Schwarz, L., Kreifelts, B., Wildgruber, D., Erb, M., Scheffler, K., and Ethofer, T. (2019). Properties of face localizer activations and their application in functional magnetic resonance imaging (fMRI) fingerprinting. PLoS One *14*, e0214997. 10.1371/journal.pone.0214997.

36. Tanaka, J.W. (2001). The entry point of face recognition: evidence for face expertise. J Exp Psychol Gen *130*, 534-543. 10.1037//0096-3445.130.3.534.

37. Yue, X., Robert, S., and Ungerleider, L.G. (2020). Curvature processing in human visual cortical areas. Neuroimage *222*, 117295. 10.1016/j.neuroimage.2020.117295.

38. Taubert, J., Wardle, S.G., and Ungerleider, L.G. (2020). What does a "face cell" want?'. Prog Neurobiol *195*, 101880. 10.1016/j.pneurobio.2020.101880.

39. Dawel, A., Krumhuber, E.G., and Palermo, R. (2025). Faking It Isn't Making It: Research Needs Spontaneous and Naturalistic Facial Expressions. Affective Science. 10.1007/s42761-025-00320-1.

40. Long, H., Peluso, N., Baker, C.I., Japee, S., and Taubert, J. (2023). A database of heterogeneous faces for studying naturalistic expressions. Sci Rep *13*, 5383. 10.1038/s41598-023-32659-5.

41. Taubert, J., and Japee, S. (2024). Real Face Value: The Processing of Naturalistic Facial Expressions in the Macaque Inferior Temporal Cortex. J Cogn Neurosci, 1-17. 10.1162/jocn_a_02108.

42. Rossion, B., Torfs, K., Jacques, C., and Liu-Shuang, J. (2015). Fast periodic presentation of natural images reveals a robust face-selective electrophysiological response in the human brain. J Vis *15*, 15.11.18. 10.1167/15.1.18.

43. Peluso, N., Saurels, B.W., and Taubert, J. (2025). Toward ecological validity in expression discrimination: Forced-choice saccadic responses to posed and naturalistic faces. Emotion. 10.1037/emo0001527.

44. Russ, B.E., and Leopold, D.A. (2015). Functional MRI mapping of dynamic visual features during natural viewing in the macaque. NeuroImage *109*, 84-94. 10.1016/j.neuroimage.2015.01.012.

45. Bainbridge, W.A., and Baker, C.I. (2020). Boundaries Extend and Contract in Scene Memory Depending on Image Properties. Curr Biol *30*, 537-543.e533. 10.1016/j.cub.2019.12.004.

46. Robinson, A.K., Stuart, G., Shatek, S.M., Herbert, A., and Taubert, J. (2025). Neural correlates reveal separate stages of spontaneous face perception. Commun Psychol *3*, 126. 10.1038/s44271-025-00308-4.

47. Teichmann, L., Hebart, M.N., and Baker, C.I. (2025). Dynamic representation of multidimensional object properties in the human brain. bioRxiv. 10.1101/2023.09.08.556679.

48. Robinson, A.K., Stuart, G., Shatek, S.M., Herbert, A., and Taubert, J. (2025). How the spontaneous perception of face pareidolia unfolds over time. PsyArXiv Preprints. https://osf.io/preprints/psyarxiv/vrtbx_v1.

49. Hebart, M.N., Zheng, C.Y., Pereira, F., and Baker, C.I. (2020). Revealing the multidimensional mental representations of natural objects underlying human similarity judgements. Nat Hum Behav *4*, 1173-1185. 10.1038/s41562-020-00951-3.

50. Afraz, S.R., Kiani, R., and Esteky, H. (2006). Microstimulation of inferotemporal cortex influences face categorization. Nature *442*, 692-695. 10.1038/nature04982.

51. Ohayon, S., Freiwald, W.A., and Tsao, D.Y. (2012). What makes a cell face selective? The importance of contrast. Neuron *74*, 567-581. 10.1016/j.neuron.2012.03.024.

52. Rhodes, G. (1985). Lateralized processes in face recognition. Br J Psychol *76 (Pt 2)*, 249-271. 10.1111/j.2044-8295.1985.tb01949.x.

53. Duchaine, B., and Yovel, G. (2015). A Revised Neural Framework for Face Processing. Annu Rev Vis Sci *1*, 393-416. 10.1146/annurev-vision-082114-035518.

54. Rossion, B., and Lochy, A. (2022). Is human face recognition lateralized to the right hemisphere due to neural competition with left-lateralized visual word recognition? A critical review. Brain Struct Funct *227*, 599-629. 10.1007/s00429-021-02370-0.

55. Goold, J.E., and Meng, M. (2017). Categorical learning revealed in activity pattern of left fusiform cortex. Hum Brain Mapp *38*, 3648-3658. 10.1002/hbm.23620.

56. Brunamonti, E., and Paré, M. (2023). Neuronal activity in posterior parietal cortex area LIP is not sufficient for saccadic eye movement production. Front Integr Neurosci *17*, 1251431. 10.3389/fnint.2023.1251431.

57. Liu, N., Avidan, G., Turchi, J.N., Hadj-Bouziane, F., and Behrmann, M. (2024). A Possible Neural Basis for Attentional Capture of Faces Revealed by Functional Magnetic Resonance Imaging and Causal Pharmacological Inactivation in Macaques. Journal of Cognitive Neuroscience *36*, 2761-2779. 10.1162/jocn_a_02211.

58. Bisley, J.W., and Goldberg, M.E. (2003). The role of the parietal cortex in the neural processing of saccadic eye movements. Adv Neurol *93*, 141-157.

59. Wardak, C., Olivier, E., and Duhamel, J.R. (2004). A deficit in covert attention after parietal cortex inactivation in the monkey. Neuron *42*, 501-508. 10.1016/s0896-6273(04)00185-0.

60. Kämmer, L., Kroell, L.M., Knapen, T., Rolfs, M., and Hebart, M.N. (2025). Decoding peripheral saccade targets from foveal retinotopic cortex. bioRxiv, 2025.2002.2020.639262. 10.1101/2025.02.20.639262.

61. Yetter, M., Robert, S., Mammarella, G., Richmond, B., Eldridge, M.A.G., Ungerleider, L.G., and Yue, X. (2021). Curvilinear features are important for animate/inanimate categorization in macaques. J Vis *21*, 3. 10.1167/jov.21.4.3.

62. Kelley, W.M., Macrae, C.N., Wyland, C.L., Caglar, S., Inati, S., and Heatherton, T.F. (2002). Finding the self? An event-related fMRI study. J Cogn Neurosci *14*, 785-794. 10.1162/08989290260138672.

63. Mitchell, J.P., Macrae, C.N., and Banaji, M.R. (2006). Dissociable medial prefrontal contributions to judgments of similar and dissimilar others. Neuron *50*, 655-663. 10.1016/j.neuron.2006.03.040.

64. Azadi, R., Lopez, E., Taubert, J., Patterson, A., and Afraz, A. (2024). Inactivation of face-selective neurons alters eye movements when free viewing faces. Proc Natl Acad Sci U S A *121*, e2309906121. 10.1073/pnas.2309906121.

65. Simpson, E.A., Maylott, S.E., Mitsven, S.G., Zeng, G., and Jakobsen, K.V. (2020). Face detection in 2- to 6-month-old infants is influenced by gaze direction and species. Dev Sci *23*, e12902. 10.1111/desc.12902.

66. Leopold, D.A., and Park, S.H. (2020). Studying the visual brain in its natural rhythm. Neuroimage *216*, 116790. 10.1016/j.neuroimage.2020.116790.

67. Wardle, S.G., and Baker, C. (2020). Recent advances in understanding object recognition in the human brain: deep neural networks, temporal dynamics, and context. F1000Res *9*. 10.12688/f1000research.22296.1.

68. Liu, T.T., Fu, J.Z., Chai, Y., Japee, S., Chen, G., Ungerleider, L.G., and Merriam, E.P. (2022). Layer-specific, retinotopically-diffuse modulation in human visual cortex in response to viewing emotionally expressive faces. Nature communications *13*, 6302. 10.1038/s41467-022-33580-7.

69. Williams, M.A., Baker, C.I., Op de Beeck, H.P., Shim, W.M., Dang, S., Triantafyllou, C., and Kanwisher, N. (2008). Feedback of visual object information to foveal retinotopic cortex. Nat Neurosci *11*, 1439-1445. 10.1038/nn.2218.

70. Leopold, D.A., Mitchell, J.F., and Freiwald, W.A. (2020). Chapter 25 - Evolved Mechanisms of High-Level Visual Perception in Primates. In Evolutionary Neuroscience (Second Edition), J.H. Kaas, ed. (Academic Press), pp. 589-625. https://doi.org/10.1016/B978-0-12-820584-6.00025-8.

71. Rossion, B., and Taubert, J. (2019). What can we learn about human individual face recognition from experimental studies in monkeys? Vision Res *157*, 142-158. 10.1016/j.visres.2018.03.012.

72. Rossion, B., and Taubert, J. (2017). Commentary: The Code for Facial Identity in the Primate Brain. Front Hum Neurosci *11*, 550. 10.3389/fnhum.2017.00550.

73. Yovel, G., and Freiwald, W.A. (2013). Face recognition systems in monkey and human: are they the same thing? F1000Prime Rep *5*, 10. 10.12703/p5-10.

74. Rossion, B. (2018). Damasio's error - Prosopagnosia with intact within-category object recognition. J Neuropsychol *12*, 357-388. 10.1111/jnp.12162.

75. Sergent, J., and Signoret, J.L. (1992). Varieties of functional deficits in prosopagnosia. Cereb Cortex *2*, 375-388. 10.1093/cercor/2.5.375.

76. Barton, J.J. (2008). Structure and function in acquired prosopagnosia: lessons from a series of 10 patients with brain damage. J Neuropsychol *2*, 197-225. 10.1348/174866407x214172.

77. Ellis, H.D., and Lewis, M.B. (2001). Capgras delusion: a window on face recognition. Trends in Cognitive Sciences *5*, 149-156. https://doi.org/10.1016/S1364-6613(00)01620-X.

78. Martens, M.A., Wilson, S.J., Dudgeon, P., and Reutens, D.C. (2009). Approachability and the amygdala: insights from Williams syndrome. Neuropsychologia *47*, 2446-2453. 10.1016/j.neuropsychologia.2009.04.017.

79. Herrington, J.D., Taylor, J.M., Grupe, D.W., Curby, K.M., and Schultz, R.T. (2011). Bidirectional communication between amygdala and fusiform gyrus during facial recognition. Neuroimage *56*, 2348-2355. 10.1016/j.neuroimage.2011.03.072.

80. Kann, S.J., O'Rawe, J.F., Huang, A.S., Klein, D.N., and Leung, H.C. (2017). Preschool negative emotionality predicts activity and connectivity of the fusiform face area and amygdala in later childhood. Soc Cogn Affect Neurosci *12*, 1511-1519. 10.1093/scan/nsx079.

81. Sawada, M., Adolphs, R., Dlouhy, B.J., Jenison, R.L., Rhone, A.E., Kovach, C.K., Greenlee, J.D.W., Howard Iii, M.A., and Oya, H. (2022). Mapping effective connectivity of human amygdala subdivisions with intracranial stimulation. Nat Commun *13*, 4909. 10.1038/s41467-022-32644-y.

82. McFadyen, J., Mattingley, J.B., and Garrido, M.I. (2019). An afferent white matter pathway from the pulvinar to the amygdala facilitates fear recognition. Elife *8*. 10.7554/eLife.40766.

83. Tsao, D.Y., and Livingstone, M.S. (2008). Mechanisms of face perception. Annu Rev Neurosci *31*, 411-437. 10.1146/annurev.neuro.30.051606.094238.

84. Ming-Hsuan, Y., Kriegman, D.J., and Ahuja, N. (2002). Detecting faces in images: a survey. IEEE Transactions on Pattern Analysis and Machine Intelligence *24*, 34-58. 10.1109/34.982883.

85. Viola, P., and Jones, M. (2001). Rapid object detection using a boosted cascade of simple features. 8-14 Dec. 2001. pp. I-I.

86. Crawford, K., and Paglen, T. (2019). Excavating AI: The Politics of Training Sets for Machine Learning Published online September 19, 2019.

87. Rekow, D., Baudouin, J.Y., Poncet, F., Damon, F., Durand, K., Schaal, B., Rossion, B., and Leleu, A. (2021). Odor-driven face-like categorization in the human infant brain. Proc Natl Acad Sci U S A *118*. 10.1073/pnas.2014979118.

88. Wardle, S.G., Taubert, J., Teichmann, L., and Baker, C.I. (2020). Rapid and dynamic processing of face pareidolia in the human brain. Nat Commun *11*, 4518. 10.1038/s41467-020-18325-8.

89. Flessert, M., Taubert, J., and Beran, M.J. (2022). Assessing the perception of face pareidolia in children (Homo sapiens), rhesus monkeys (Macaca mulatta), and capuchin monkeys (Sapajus apella). Journal of comparative psychology (Washington, D.C. : 1983). 10.1037/com0000320.

90. Jakobsen, K.V., Hunter, B.K., and Simpson, E.A. (2023). Pareidolic faces receive prioritized attention in the dot-probe task. Atten Percept Psychophys. 10.3758/s13414-023-02685-6.

91. Sharma, S., Vinken, K., and Livingstone, M.S. (2023). When the whole is only the parts: non-holistic object parts predominate face-cell responses to illusory faces. bioRxiv. 10.1101/2023.09.22.558887.

92. Lipp, O.V., and Taubert, J. (2024). The face pareidolia illusion drives a happy face advantage that is dependent on perceived gender. Emotion. 10.1037/emo0001346.

93. Koyano, K.W., Taubert, J., Robison, W., Waidmann, E.N., and Leopold, D.A. (2025). Face pareidolia minimally engages macaque face selective neurons. Prog Neurobiol *245*, 102709. 10.1016/j.pneurobio.2024.102709.

94. Hamilton, M., Stent, S., DuTell, V., Harrington, A., Corbett, J., Rosenholtz, R., and Freeman, W.T. (2024). Seeing Faces in Things: A Model and Dataset for Pareidolia.

95. Gupta, P., and Dobs, K. (2025). Human-like face pareidolia emerges in deep neural networks optimized for face and object recognition. PLoS Comput Biol *21*, e1012751. 10.1371/journal.pcbi.1012751.

96. Nicholls, M.E., Thomas, N.A., Loetscher, T., and Grimshaw, G.M. (2013). The Flinders Handedness survey (FLANDERS): a brief measure of skilled hand preference. Cortex; a journal devoted to the study of the nervous system and behavior *49*, 2914-2926. 10.1016/j.cortex.2013.02.002.

97. Kriegeskorte, N., Mur, M., and Bandettini, P. (2008). Representational similarity analysis - connecting the branches of systems neuroscience. Front Syst Neurosci *2*, 4. 10.3389/neuro.06.004.2008.

98. Stuart, G., Saurels, B.W., Robinson, A.K., and Taubert, J. (2025). One object with two identities: The rapid detection of face pareidolia in face and food detection tasks. J Exp Psychol Hum Percept Perform *51*, 710-720. 10.1037/xhp0001296.

99. Xiao, J., Hays, J., Ehinger, K.A., Oliva, A., and Torralba, A. (2010). SUN database: Large-scale scene recognition from abbey to zoo. 13-18 June 2010. pp. 3485-3492.

100. Grootswagers, T., Robinson, A.K., Shatek, S.M., and Carlson, T.A. (2024). Mapping the dynamics of visual feature coding: Insights into perception and integration. PLoS Comput Biol *20*, e1011760. 10.1371/journal.pcbi.1011760.

101. de Leeuw, J.R. (2015). jsPsych: a JavaScript library for creating behavioral experiments in a Web browser. Behav Res Methods *47*, 1-12. 10.3758/s13428-014-0458-y.

102. Peirce, J., Gray, J.R., Simpson, S., MacAskill, M., Höchenberger, R., Sogo, H., Kastman, E., and Lindeløv, J.K. (2019). PsychoPy2: Experiments in behavior made easy. Behav Res Methods *51*, 195-203. 10.3758/s13428-018-01193-y.

103. Stigliani, A., Weiner, K.S., and Grill-Spector, K. (2015). Temporal Processing Capacity in High-Level Visual Cortex Is Domain Specific. J Neurosci *35*, 12412-12424. 10.1523/jneurosci.4822-14.2015.

104. Cox, R.W. (1996). AFNI: software for analysis and visualization of functional magnetic resonance neuroimages. Computers and biomedical research, an international journal *29*, 162-173. 10.1006/cbmr.1996.0014.

105. Cox, R.W., and Hyde, J.S. (1997). Software tools for analysis and visualization of fMRI data. NMR Biomed *10*, 171-178. 10.1002/(sici)1099-1492(199706/08)10:4/5<171::aid-nbm453>3.0.co;2-l.

106. Saad, Z.S., Reynolds, R.C., Argall, B., Japee, S., and Cox, R.W. (2004). SUMA: an interface for surface-based intra- and inter-subject analysis with AFNI. 18-18 April 2004. pp. 1510-1513 Vol. 1512.

107. Saad, Z.S., Glen, D.R., Chen, G., Beauchamp, M.S., Desai, R., and Cox, R.W. (2009). A new method for improving functional-to-structural MRI alignment using local Pearson correlation. Neuroimage *44*, 839-848. 10.1016/j.neuroimage.2008.09.037.

108. RW, C., and DR, G. (2013). Nonlinear warping in AFNI. . Presented at the 19th Annual Meeting of the Organization for Human Brain Mapping.

109. Fonov, V.S., Evans, A.C., McKinstry, R.C., Almli, C.R., and Collins, D.L. (2009). Unbiased nonlinear average age-appropriate brain templates from birth to adulthood. NeuroImage *47*, S102. https://doi.org/10.1016/S1053-8119(09)70884-5.

110. Fonov, V., Evans, A.C., Botteron, K., Almli, C.R., McKinstry, R.C., and Collins, D.L. (2011). Unbiased average age-appropriate atlases for pediatric studies. NeuroImage *54*, 313-327. https://doi.org/10.1016/j.neuroimage.2010.07.033.

111. Reynolds, R.C., Glen, D.R., Chen, G., Saad, Z.S., Cox, R.W., and Taylor, P.A. (2024). Processing, evaluating, and understanding FMRI data with afni_proc.py. Imaging Neurosci (Camb) *2*, 1-52. 10.1162/imag_a_00347.

112. Hebart, M.N., Görgen, K., and Haynes, J.D. (2014). The Decoding Toolbox (TDT): a versatile software package for multivariate analyses of functional imaging data. Frontiers in neuroinformatics *8*, 88. 10.3389/fninf.2014.00088.